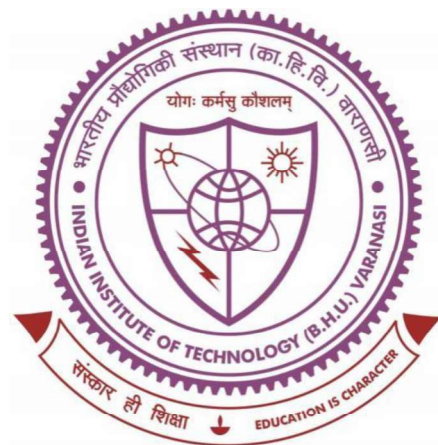


Development of Water Soluble, White Light Generating Highly Biocompatible Lanthanide Oxide Nanoparticles for Applications in Health Care.



Thesis submitted in partial fulfillment

For the Award of Degree

Doctor of Philosophy

BY

VIVEK KUMAR VERMA

SCHOOL OF BIOMEDICAL ENGINEERING

INDIAN INSTITUTE OF TECHNOLOGY BHU, VARANASI, 221005, U.P.,
INDIA



Dedication

*I am dedicating this Ph.D. thesis to my family and the people of my country,
India, who paid for the cost of this study.*





भारतीय
प्रौद्योगिकी
संस्थान
काशी हिन्दू विश्वविद्यालय



INDIAN
INSTITUTE OF
TECHNOLOGY
BANARAS HINDU UNIVERSITY

CERTIFICATE

It is certified that the work contained in the thesis titled “**Development of Water Soluble, White Light Generating Highly Biocompatible Lanthanide Oxide Nanoparticles for Applications in Health Care**” by **Vivek Kumar Verma** has been carried out under my supervision and that this work has not been submitted elsewhere for a degree.

It is further certified that the student has fulfilled all the requirements of Comprehensive Examination, Candidacy, and SOTA for the award of Ph.D. Degree.

Dr. Manoj Kumar

(Supervisor)

Department of Chemical Engineering & Technology,
Indian Institute of Technology,
(Banaras Hindu University),

Varanasi-221005, India
Dr. MANOJ KUMAR
Associate Professor
Department of Chemical Engg. & Techn.
IIT (BHU), Varanasi-221005



भारतीय
प्रौद्योगिकी
संस्थान
काशी हिन्दू विश्वविद्यालय



INDIAN
INSTITUTE OF
TECHNOLOGY
BANARAS HINDU UNIVERSITY

DECLARATION BY THE CANDIDATE

I, Vivek Kumar Verma, certify that the work embodied in this Ph.D. thesis is my own bonafide work and was carried out by me under the supervision of **Dr. Manoj Kumar** for a period from **July 2018 to September 2023** at the School of Biomedical Engineering, Indian Institute of Technology (Banaras Hindu University), Varanasi. The matter embodied in this thesis has not been submitted for the award of any other degree/diploma. I declare that I have faithfully acknowledged and given credit to the research workers wherever their works have been cited in my work in this thesis. I further declare that I have not wilfully copied any other's work, paragraph, text, data, results, etc. reported in the journals, books, magazines, reports, dissertations, thesis, etc., or available on websites and have not included in this thesis and have not cited as my own work.

Date: 19/09/2023

Place: IIT (BHU), Varanasi

Vivek Kumar Verma

CERTIFICATE FROM THE SUPERVISOR

It is certified that the above statement made by the student is correct to the best of my knowledge.

Dr. Manoj Kumar

(Supervisor)

Department of Chemical Engineering & Technology,
Indian Institute of Technology,
(Banaras Hindu University),
Varanasi-221005, India
Dr. MANOJ KUMAR
Associate Professor
Department of Chemical Engg. & Techn.
IIT (BHU), Varanasi-221005

Coordinator of the School

समन्वयक/CO-ORDINATOR

जैव चिकित्सा अभियांत्रिकी स्कूल
SCHOOL OF BIOMEDICAL ENGG
भारतीय प्रौद्योगिकी संस्थान (का.हि.वि.)
INDIAN INSTITUTE OF TECHNOLOGY (B.H.U.)
वाराणसी 221005/VARANASI-221005

COPYRIGHT TRANSFER CERTIFICATE

Title of Thesis: **“Development of Water Soluble, White Light Generating Highly Biocompatible Lanthanide Oxide Nanoparticles for Applications in Health Care”**

Candidate's Name: **Vivek Kumar Verma**

Copyright Transfer

The undersigned hereby assigns to the Indian Institute of Technology (Banaras Hindu University) Varanasi all rights under copyright that may exist in and for the above thesis submitted for the award of the Doctor of Philosophy degree.

Date: 22/09/2023

Place: IIT (BHU), Varanasi



(Vivek Kumar Verma)

Note: However, the author may reproduce or authorize others to reproduce material extracted verbatim from the thesis or derivative of the thesis for the author's personal use, provided that the source and the Institute's copyright notice are indicated.

ACKNOWLEDGMENT

It's a great occasion to thank my esteemed supervisor, **Dr. Manoj Kumar**, Associate Professor, Department of Chemical Engineering & Technology, IIT (BHU) Varanasi, for his constant cheer, support, and cooperation. His helping nature and proper guidance created a healthy research environment around me, which helped significantly improve my technical writing and presentation skills besides completing the research objectives.

I express my sincere gratitude to **Dr. Pradeep Paik** (School of Biomedical Engineering, IIT BHU) and **Dr. Avanish Singh Parmar** of Applied Physics Department, IIT (BHU), for being part of my research progress evaluation committee. Their constructive guidance, encouragement, and moral support throughout my doctoral work helped me achieve the thesis objectives.

I am also expressing my sincere thanks to **Dr. Ashutosh Dubey** from the Department of Ceramic Engineering, IIT BHU, for their constructive criticism and valuable suggestions during my research work.

I am also thankful to **Dr. Amit Prabhakar** and **Dr. Amaresh Kumar Sahoo** of the Department of Applied Science, IIIT-Allahabad, for their unparalleled supervision during my undergraduate and master's degree program from the Department of Applied Science, IIIT-Allahabad. He always made time to listen and provide cautious advice whenever I needed it.

I owe my thanks to **Prof. Sanjeev Kumar Mahto** (coordinator), School of Biomedical Engineering, and **Prof. M.K Mondal** (Head), Department of Chemical Engineering & Technology, IIT (BHU) for encouraging and providing me with all the facilities to carry out my research work.

I would like to sincerely thank all **DPGC** members for their direct or indirect motivation and assistance from different corners during my research work at the institute. Also, I express my sincere thanks to all **faculty members** and **non-teaching staff** of the School of Biomedical Engineering and the Department of Chemical Engineering and Technology, Indian Institute of Technology (BHU), for their continued help and cooperation in completing this dissertation work.

I thank my seniors, **Shivesh Sabbarawal** and **Dr. Kedar Sahoo** for their sincere guidance, cooperation, and motivation during the entire thesis work.

A special thanks to **Ms. Prachi Srivastava** for her incredible continuous support during my entire Ph.D. duration.

I am also thankful to all my lab mates, **Mr. Anshuman Singh** and **Ms. Rinki Verma**, for their valuable help and moral support throughout this journey.

I would like to express my deepest and most heartfelt thanks to my friends **Abhishesh Kumar Mehta**, **Deepa Dehari** and **Bindu Kumari**, **Saurabh Jauhari**, **Himanshu Kumar**, and **Chakshu Bhatiya**; they have always been a source of inspiration for me and have stood by my side at the most challenging times.

I acknowledge the **Ministry of Human Resource Development (MHRD)**, **New Delhi, India**, for their time-to-time financial support during my stay at **IIT (BHU)**.

I am also grateful to the **Department of Science & Technology** under the **Ministry of Science & Technology** of the **Government of India** for providing financial aid for fuelling the research.

I am also thankful to the **Indian Institute of Technology (BHU) Varanasi, India**, for providing the laboratory and research facility during my Ph.D. tenure.

Last but not least, I am highly obliged to my Parents **Mr. Shashi Kant Verma** and **Mrs. Vindhyawashani Verma** with my brother **Vishesh Kumar Verma** and Sisters **Pallavi Verma**, **Preeti Verma**. Their motivation, encouragement, and backing throughout my entire career till the completion of my Ph.D. mean a lot to me.

Date: 22/09/2023

Place: IIT (BHU), Varanasi

(**Vivek Kumar Verma**)

Table of Contents

Page No.

Certificate.....	iii
Declaration by the candidate and certificate by the supervisor.....	iv
Copyright transfer certificate.....	v
Acknowledgment.....	vi-vii
Table of contents.....	viii-xii
List of figures.....	xiii-xviii
List of tables	xix
List of Abbreviations.....	xx-xxi
Preface	xxii-xxiv
Chapter 1 Introduction.....	1-36
1.1 Introduction.....	1-5
1.2 Cancer:A Group of Disease.....	5-7
1.3 Multimodal Cancer Imaging.....	7-10
1.4 Fluorescence Bio-Imaging.....	10-11
1.4.1 Size effect of nanomaterial for Bioimaging.....	11-12
1.5 Fluorescence -imaging-based cancer therapy.....	12-13
1.5.1 Fluorescence imaging in drug delivery (Theranostic).....	12-13
1.5.2 Fluorescence imaging-guided surgery.....	13-14
1.6 Magnetic Resonance Imaging (MR- Imaging)	15-16
1.6.1 Working Principle of MRI.....	15-17
1.6.2 T1-Weighted Relaxation Process (Longitudinal Relaxation).....	17-18
1.6.3 T2-Weighted Relaxation Process (Transvers Relaxations	18-19
1.7 MRI contrast agents	19-22
1.8 Gadolinium as Positive Contrast Agent.....	22-24
1.9 Gadolinium Oxide as a Dual Modalities.....	24-31
1.9.1 Various Synthesis Route of Gd ₂ O ₃ Nanomaterial.....	5-26
1.9.2 Chemical Reduction Method	27-27
1.9.3 Hydrothermal Method.....	27-28
1.9.4 Microwave-Assisted Synthesis.....	28-29
1.9.5 Biomineralization Encourages Synthesis.....	29-30

1.9.6 Sol-Gel Method.....	31
1.10 Functionalization of Gd ₂ O ₃ nanomaterial.....	31-34
1.10.1 Citric acid.....	32
1.10.2 Polyethylene glycol (PEG).....	32
1.10.3 Polyvinylpyrrolidone (PVP).....	33
1.10.4 Silica (SiO ₂)	33
1.10.5 Antibodies or peptides	34
1.11 Problem statement	35-36
Chapter 2 Literature review.....	37-60
2.2 Development of Gd ₂ O ₃ nanomaterial.....	38-43
2.3 Texture, Shape, and Size Effect on Gadolinium Oxide Nanoparticle on Properties.....	44-47
2.3.1 Porous Sheet-like Particles.....	44-45
2.3.1 Nanodisks.....	45
2.3.3 Spherical NPs.....	45
2.3.4 Rod Shaped.....	45-47
2.3.5 Nanofiber.....	46-47
2.4 Thermogravimetric study of Gd ₂ O ₃	47-53
2.4.1 Non iso-conversional method to compute activation energy	48-49
2.4.2 Thermodynamics parameter calculation.....	49
2.4.3 Computation of nucleation rate and interfacial energy of nanomaterial	50-53
2.5 General Biological Applications of Gadolinium Oxide NPs	53-57
2.5.1 Multimodal imaging.....	54-55
2.5.2 Antibacterial.....	56
2.5.3 Drug delivery.....	56-57
Aim and Objective of the current work.....	58-60
Chapter 3 Fluorescent Gadolinium Oxide Nanoclusters.....	61-90
3.1 Introduction.....	61-65
3.2 Experimental Section	65-66
3.2.1 Chemicals	65
3.2.2 Synthesis of Gd ₂ O ₃ Nanoclusters.....	65-66
3.3 Characterization	66-70
3.3.1 Transmission Electron Microscopy (TEM).....	66

3.3.2 Fluorescence Spectroscopy.....	67
3.3.3 UV-Vis Spectroscopy.....	67
3.3.4 Fourier Transform Infrared (FTIR) spectroscopy.....	67
3.3.5 X-ray diffraction (XRD).....	67
3.3.6 X-ray photoelectron spectra (XPS).....	67
3.3.7 Matrix-Assisted Laser Desorption Ionization Time-of-Flight (MALDI-TOF).....	67-68
3.3.8 Fluorescence Life Time Decay Analysis.....	68
3.3.9 Cell Culture and Cell Viability Assay.....	68-69
3.3.10 Confocal Microscopy.....	69
3.3.11 Quantum Yield Measurement.....	69-70
3.4 Result and discussion.....	70-90
3.4.1 Applications of Gd ₂ O ₃ Nanoclusters	86-89
3.4.2 In-vitro imaging of Gd ₂ O ₃ in HaCaT cell line.....	89-90
Chapter 4 Nucleation Rate & Interfacial Energy for Gd₂O₃ Nanoclusters.....	91-120
4.1 Introduction.....	91-95
4.2 Computation and theoretical background with determination kinetics parameters.....	95-97
4.2.1 Thermogravimetric Analysis.....	95
4.2.2 Kinetic Parameter.....	95-97
4.3 Iso-conversional model (model-free).....	97-100
4.3.1 Ozawa Wall Flynn (FWO) method	97
4.3.2 The Kissinger Akhira Sunose (KAS) method.....	97-98
4.3.3 Starink method.....	98
4.3.4 Tang method.....	89-99
4.3.5 Vyazovkin.....	99
4.3.6 Vyazovkin AIC.....	99-100
4.4 Interpretation of Pre exponential kinetic factor and Thermodynamic barriers of random nucleation in Gd ₂ O ₃ NCs.....	100-101
4.5 Interpretation of nucleation rate as a function of Interfacial energy, Thermodynamic, and Kinetic factors	101-102
4.6 Experimental sections.....	102-103
4.6.1 Chemicals se.....	102
4.6.2 Synthesis of Gd ₂ O ₃ NCs.....	102-103

4.7 Characterization	105
4.8 Results and discussion	103-120
4.8.1 UV-Vis spectroscopy.....	103-104
4.8.2 Infrared Spectroscopy and Surface Analysis.....	104
4.8.3 Size and phase analysis.....	105-106
4.8.4 Determination of Reaction kinetics model and pathways.....	107-108
4.8.5 Estimation of apparent value of activation energy concerning reaction progression.....	108-111
4.8.6 Interrogation of TGA/DTG curve.....	111-112
4.8.7 Calculation of Pre-exponential factor (Aa) as a function of conversion.....	113
4.8.8 Computation of Thermodynamic parameters for reaction progression....	114-118
4.8.9 Variation in rate of nucleation concerning conversion and temperature...	118-119
4.8.10 Variation in interfacial energy with respect to conversion and temperature	119-120
Chapter 5 Multimodal Imaging of Gadolinium Oxide Nanoclusters	123-152
5.1 Introduction.....	123-125
5.2 Experimental Section	125-131
5.2.1 Chemicals Used.....	125
5.2.2 Synthesis procedur	125-126
5.2.3 Characterization.....	126
5.2.4 Cytotoxicity estimation.....	127
5.2.5 Hemocompatibility assay.....	127-128
5.2.6 Histopathology in rat.....	128-129
5.2.7 Clinical signs and body weight measurement	129
5.2.8 In vivo biodistribution and fluorescence signal in the healthy Rat after Gd ₂ O ₃ NCs administration.....	129
5.2.9 Absolute Quantum Yield Measurement.....	129-130
5.2.10 Relaxivity Measurement	130-131
5.3 Results and Discussion.....	131-152
5.3.1 Fluorescence spectroscopy and UV–Vis spectroscopic characterization..	131-132
5.3.2 Size and phase analysis.....	133-134
5.3.3 Surface and Infrared Spectroscopy.....	134-137
5.3.4 Stability of Gd ₂ O ₃ nanocluster	138

5.3.5 Mechanism behind synthesis	139-140
5.4 Application of Gd ₂ O ₃ nanoclusters.....	140-152
5.4.1 Biocompatibility.....	140-141
5.4.2 In-vitro cytocompatibility (MTT assay)	141
5.4.3 Hemocompatibility assay.....	141
5.4.4 In-vivo Cytocompatibility test.....	142
5.4.5 In-vitro cell imaging.....	144
5.4.6 Z stacking (focus stacking) Confocal Analysis	145-149
5.4.7 In-vivo imaging system (IVIS imaging)	150-151
5.4.8 Relaxivities Measurement	152
Chapter 6 Conclusion and future work	153-156
6.1 Conclusion	153-155
6.2 Future work.....	155-156
References.....	157-192
Appendix.....	193-210
Publications.....	211-213
Permission from Central Ethical Committee.....	214

LIST OF FIGURES

Figure no.	Figure caption	Page no.
Figure 1.1	Cancer cell proliferation mechanism from a normal cell	6
Figure 1.2	Possible imaging modalities with their advantage used in optical imaging	10
Figure 1.3	Basic fluorescence detection setup for nanomaterials	13
Figure 1.4	Basic fluorescence mechanism in tissue tagged through fluorophore agents	14
Figure 1.5	The net magnetization (M) is a vector that can be split into longitudinal (M_z) and transverse (M_{xy}) components relative to the principal magnetic field (B_0)	17
Figure 1.6	Schematic diagram of the NMR technique test mechanism	17
Figure 1.7	The T1 relaxation process is the return of the net magnetization (M) to its initial maximal value (M_0)	18
Figure 1.8	Transverse relaxation processes (T2) A diagram illustrating the process of transverse relaxation following the application of a 90° RF pulse at equilibrium.	19
Figure 1.9	The diagram shows that the contrast agents bind to the aggressive tumor and give significant single	20
Figure 1.10	Pre- and post-gadolinium-based contrast agent T1 weighted image from malignant tumor patient	21
Figure 1.11	Commercially available gadolinium-based contrast agents with their structure	23
Figure 1.12	Synthesis mechanism of biocompatible gadolinium oxide nanomaterials with different polymers in possible fluorescent imaging and MR imaging	25
Figure 1.13	Top-down and bottom-up approach for the synthesis of nanomaterials	26
Figure 1.14	The mechanism for the synthesis of nanomaterials using the chemical reduction method	27
Figure 1.15	Hydrothermal approaches to the synthesis of nanomaterials with different shapes	28
Figure 1.16	Microwave-assisted synthesis of nanomaterials	29

Figure 1.17	Biom mineralization Encourage Synthesis of nanomaterials using different plant extracts or microorganisms like fungi, bacteria, and yeast	30
Figure 1.18	Sol-gel approach for the synthesis of nanomaterials with different disposition mechanisms	31
Figure 1.19	All plausible applications for gadolinium-based nanomaterials functionalized with different ligands, proteins, acids and polymers	34
Figure 3.1	Optimization of incubation time at 0 hr, 15 hrs, 24 hrs, 48 hrs, 72 hrs, and 96 hrs of the Gd ₂ O ₃ nanoclusters at particular excitation of (a) 366 nm, (b) 469 nm, (c) 516 nm, and (d) 560 nm.	71
Figure 3.2	The fluorescence emission spectra of Gd ₂ O ₃ nanoclusters and its controls (Gd salt + BSA) and (Gd salt + ascorbic acid) (a) The optimal excitation-emission spectra of Gd ₂ O ₃ nanoclusters and controls at Ex- 366 / Em- 465 (b) The optimal excitation-emission spectra of Gd ₂ O ₃ nanoclusters and controls at Ex- 469 / Em- 546 (c) The optimal excitation-emission spectra of Gd ₂ O ₃ nanoclusters and controls at Ex- 516 / Em- 595 (d) The optimal excitation-emission spectra of Gd ₂ O ₃ nanoclusters and controls at Ex- 560 /Em- 615	73
Figure 3.3	(a) Normalized fluorescent spectra of Gd ₂ O ₃ nanoclusters at excitation 300 nm, (b) CIE 1931 chromaticity diagram for Gd ₂ O ₃ nanoclusters with coordinate (0.33,0.37) which nearly by ideal white light coordinate (0.33,0.33), (c) Excitation wavelength dependent normalized 3D fluorescent intensity spectra, (d) White light Emission of Gd ₂ O ₃ nanoclusters under excitation.	75
Figure 3.4	Fluorescent intensity decay lifetime spectra of Gd ₂ O ₃ nanoclusters with IRF (Instrument response function) (a) Ex- 496 nm / Em- 564 nm, (b) Ex- 598 nm /Em- 658 nm. Fluorescent intensity decay lifetime spectra of incubated BSA (c) Ex- 496 nm /Em- 564 nm, (d) Ex - 598 nm / Em- 658 nm	76
Figure 3.5	(a) Lifetime decay spectra for Gd ₂ O ₃ nanoclusters (Ex. - 375 nm; Em. - 459 nm), (b) Lifetime decay spectra for BSA protein (Ex. - 375 nm; Em. - 459 nm).	77
Figure 3.6	(a) UV spectroscopy of Gd ₂ O ₃ nanoclusters and native BSA. (b) HR-TEM image of Gd ₂ O ₃ nanoclusters. (The inset image shows a histogram distribution plot for Gd ₂ O ₃ nanoclusters, where d_{avg} is the diameter average). (c), (d) Maldi-Tof spectra of BSA protein and Gd ₂ O ₃ nanoclusters, respectively.	80
Figure 3.7	(a) HR- XRD of Gd ₂ O ₃ nanoclusters and native BSA. Full resolution XPS data (b) Survey data. (c) Gd4d, (d) O1s.	82

Figure 3.8	(a) XPS spectra of C 1s. (b) Fluorescence emission spectra of lyophilized Gd ₂ O ₃ nanoclusters powder at different excitations of 366 nm, 469 nm, 516 nm and 560 nm. (c) Fluorescence emission spectrum of Gd ₂ O ₃ nanoclusters at excitation of 516 nm after addition of freshly prepared NaCl at different concentrations of solution.	83
Figure 3.9	(a) FTIR Spectra of Gd ₂ O ₃ nanoclusters, (b) pH stability fluorescent spectra at various pH (8, 10 and 12).	84
Figure 3.10	(a) Fluorescence emission spectra of Gd ₂ O ₃ nanoclusters (Conc. 11.6 mg/ml) at excitations of 469 nm at different time intervals of 7 days, 1.1 years and 2.5 years show very eminent emission. (b) Fluorescence emission spectra of Gd ₂ O ₃ nanoclusters (Conc.11.6 mg/ml) at excitations of 516 nm at different time intervals of 7 days, 1.1 years and 2.5 years show very eminent emission.	85
Figure 3.11	(a) Plot for Direct optical band gap of Gd ₂ O ₃ nanoclusters between $(\alpha h\nu)^2$ vs. $(h\nu)$, (b) Plot for Indirect optical band gap of Gd ₂ O ₃ nanoclusters between $(\alpha h\nu)^2$ vs. $(h\nu)$.	86
Figure 3.12	(a) Quantum yield for green emission of Gd ₂ O ₃ nanoclusters with rhodamine 6G as a reference at the same absorbance (≤ 0.5), (b) Quantum yield for blue emission of Gd ₂ O ₃ nanoclusters with quinine sulfate as a reference at same absorbance (≤ 0.5). (c) Photo-stability of Gd ₂ O ₃ nanoclusters for different excitations 366,469,516 and 560 nm.	88
Figure 3.13	(a) and (b) Percentage cell viability: MTT assay histogram of Gd ₂ O ₃ nanoclusters on MDA-MB -231 and HEK-239 treated with different concentrations, respectively, (Stock concentration 35 mg/ml).	99
Figure 3.14	Multi-fluorescence confocal image of HaCaT cells treated with Gd ₂ O ₃ nanoclusters (3.5 mg/ml of stock solution), (a) Ex. /Em-366 nm/blue, (b) Ex. /Em-472 nm/green, (c) Ex. /Em-472 nm/red, (d) merged image, (e) Bright-field image.	90
Figure 4.1	(a) UV-Vis spectroscopy spectrum of Gd ₂ O ₃ nanoclusters and BSA protein. (b) Fourier transform infrared spectroscopy (FTIR) spectra for Gd ₂ O ₃ nanoclusters and BSA protein.	105
Figure 4.2	Full X-ray photoelectron spectroscopy (XPS) spectra of (a) Gd 4d, (b) C1s, and (c) O1s for prepared Gd ₂ O ₃ nanoclusters	106
Figure 4.3	(a) High-resolution Transmission electron microscopy (HR-TEM) spectrum for Gd ₂ O ₃ nanocluster, (inset: Histogram distribution for selected image) with average diameter of 0.86 ± 0.29 nm. (b) HR-XRD for prepared Gd ₂ O ₃ nanoclusters with amorphous in nature.	107

Figure 4.4	(a) $Z(\alpha)$ master plot at a different conversational point for exploring the thermal decomposition reaction mechanism at 10 °C/min, 15 °C/min, and 20 °C/min. (b) All possible apparent activation energies from an iso conversion model at all the conversion	109
Figure 4.5	Kinetic analysis of prepared Gd ₂ O ₃ nanoclusters using an iso conversational model. (a) Tang, (b) Starink,(c) KAS.(d) FWO	112
Figure 4.6	Differential thermogravimetry (DTG) and Thermogravimetry (TGA) curves of prepared Gd ₂ O ₃ nanoclusters at (a)10 °C/min, (b) 15 °C/min,(c) 20 °C/min. (d) Pre-exponential factor for each iso conversion at 10°C/min, 15°C/min, and 20°C/min	114
Figure 4.7	(a) Plot between enthalpy against conversion at 10 °C/min, 15 °C/min, and 20 °C/min, (b) Plot between Gibbs free energy against conversion at 10 °C/min, 15 °C/min, and 20 °C/min, (c) Plot between Entropy against conversion at 10 °C/min, 15 °C/min, and 20 °C/min.	116
Figure 4.8	(a) Temperature-dependent nucleation rate plot of Gd ₂ O ₃ nanoclusters, (b) Conversion-dependent nucleation rate plot of Gd ₂ O ₃ nanoclusters, (c) Conversion dependent interfacial energy plot of Gd ₂ O ₃ nanoclusters, (d) Temperature-dependent interfacial energy plot of Gd ₂ O ₃ nanoclusters.	121
Figure 5.1	The fluorescence emission spectra of Gd ₂ O ₃ NCs and all possible controls. (a) The normalized emission spectra of Gd ₂ O ₃ NCs and control at Ex- 365 / Em- 447, (b) The normalized emission spectra of Gd ₂ O ₃ NCs and control at Ex- 465 / Em- 535 (c) The normalized emission spectra of Gd ₂ O ₃ NCs and control at Ex- 550 / Em- 605. (d) UV spectroscopy of Gd ₂ O ₃ NCs and native medium molecular weight Chitosan	133
Figure 5.2	(a) Transmission Electron microscopy (TEM) image of prepared for Gd ₂ O ₃ NCs, (b) Size distribution histogram for Gd ₂ O ₃ NCs (sample size ~100), (c) XRD analysis of Gd ₂ O ₃ NCs and native Chitosan polymer	135
Figure 5.3	The XPS analysis of prepared Gd ₂ O ₃ NCs. (a) The survey graph showing the presence of carbon, oxygen, and gadolinium in the sample, (b) a detailed analysis of C1s spectra showing a strong peak at 285.9 eV corresponding to carbonyl groups (C=O) and a small peak at 287.5 eV and 284.48 due to the Sp ³ , Sp ² hybridization respectively, (b) XPS analysis for Gd4d FTIR orbital, (d) XPS analysis for O1s orbital	136
Figure 5.4	(a) FTIR spectrum analysis for prepared Gd ₂ O ₃ NCs and native Chitosan polymer, (b) Normalized photostability study for Gd ₂ O ₃ NCs emission at blue (Ex. 365), green (Ex. 465) and red (Ex. 550).	137

Figure 5.5	(a) pH. dependent normalized fluorescence emission spectra at different pH. (5.8-11) at λ_{Ex} 465 nm, (b) Normalized fluorescence emission spectra for Gd_2O_3 NCs after the addition of various concentrations of freshly prepared NaCl solution at λ_{Ex} 465, (c) Normalized fluorescence emission spectra of freshly prepared Gd_2O_3 NCs with different solvent at λ_{Ex} 465, (d) Normalized fluorescence emission spectra for freshly prepared Gd_2O_3 NCs, previous 8 months and nearly 11 months old λ_{Ex} 465.	139
Figure 5.6	(a) MTT analysis of Cell Proliferation on U-87 MG (Glioma Brain Cell), (b) Hemocompatibility test for nanoclusters with positive and negative control with Di water Saline, respectively.	142
Figure 5.7	Histopathological appearance in H & E-stained rat liver sections of all groups; (a) Real image of organ taken after 28 days of injecting nanoclusters, (b) Normal tissue without injecting nanocluster (control group); (c) Tissue appearance (3 hrs) after injecting nanocluster through tail vein injection (d) Tissue appearance (7 days) after injecting nanocluster through tail vein injection, (e) Tissue appearance (28 days) after injecting nanocluster through tail vein injection. Bar: 10 μm	143
Figure 5.8	Multifluorescent confocal imaging of U 87-MG cells treated with Gd_2O_3 NCs (1.4 mg/ml of stock solution) at different excitation of (a) Ex. /Em-366 nm/blue, (b) Ex. /Em-472 nm/green, (c) Ex. /Em-472 nm/red, (d) merged image.	145
Figure 5.9	Z stack confocal images and Mean Luminescence Intensity in U 87-MG cells for Gd_2O_3 NCs. [Ex. 366 nm, Em. Blue (477 nm)] (a) = 0 μm , (b) = 2 μm , (c) = 4 μm , (d) = 6 μm , (e) = 8 μm , (f) = 10 μm , (g) = 12 μm , (h) = 14 μm , (i) = 16 μm , (j) = 18 μm , (k) = 20 μm , (l) = 22 μm , (m) = 24 μm .	147
Figure 5.10	Z stack confocal images and Mean Luminescence Intensity in U 87-MG cells for Gd_2O_3 NCs. [Ex. 472 nm, Em. Green (541 nm)] (a) = 0 μm , (b) = 2 μm , (c) = 4 μm , (d) = 6 μm , (e) = 8 μm , (f) = 10 μm , (g) = 12 μm , (h) = 14 μm , (i) = 16 μm , (j) = 18 μm , (k) = 20 μm , (l) = 22 μm , (m) = 24 μm .	148
Figure 5.11	Z stack confocal images and Mean Luminescence Intensity in U 87-MG cells for Gd_2O_3 NCs. [Ex. 472 nm, Em. Red (636 nm)] (a) = 0 μm , (b) = 2 μm , (c) = 4 μm , (d) = 6 μm , (e) = 8 μm , (f) = 10 μm , (g) = 12 μm , (h) = 14 μm , (i) = 16 μm , (j) = 18 μm , (k) = 20 μm , (l) = 22 μm , (m) = 24 μm .	150
Figure 5.12	Live animal fluorescent images of Gd_2O_3 NCs treated Mice in different time intervals	151

Figure 5.13 T1- weighted MR images of Gd_2O_3 NCs with various concentrations (equivalent Gd concentration: 0.2, 0.3, 0.4, 0.5, 1, 1.5 mM), and linear correlation between longitudinal relaxivity $\{r_1 \text{ (ms)}\}$ with equivalent Gd concentration of Gd_2O_3 NCs.

152

LIST OF TABLES

Table no.	Table caption	Page no.
Table 1.1	Comparative details of available imaging modalities	9
Table 2.1	Summarize the synthesis method of reported Gd ₂ O ₃ NPs	42-43
Table 2.2	Relaxivities of various ligand-coated gadolinium oxide nanoparticles with their size and cell viability distribution	55
Table 3.1	Fluorescence lifetime of Gd ₂ O ₃ nanoclusters and incubated BSA	77
Table 4.1	Comparative study for activation energy using different iso-conversional models	110
Table 4.2	Thermodynamic parameters at different heating rates with correspond to each conversion point	117
Table 5.1	Rats' body weight before and after Gd ₂ O ₃ NCs administration	143
Table 5.2	Comparative table of Gd ₂ O ₃ nanoclusters along with commercially available contrast agents	152

LIST OF ABBREVIATIONS AND SYMBOLS

Abbreviation	Nomenclature
MRI	Magnetic resonance imaging
CT	Computed tomography
PET	Positron emission tomography
SPECT	Single-photon emission computed tomography
US	Ultrasound
UV	Ultraviolet
NMR	Nuclear magnetic resonance
SPIONs	Superparamagnetic iron oxide nanoparticles
SPR	Surface plasmon resonance
Gd ₂ O ₃	Gadolinium oxide
NPs	Nanoparticles
NCs	Nanoclusters
IVIS	In vivo imaging system
MALDI-TOF	Matrix-assisted laser desorption/ionization
CTCF	Corrected total cell fluorescence
QDs	Quantum dots
FRET	Förster resonance energy transfer
BSA	Bovine albumin serum
WLE	White light emission
CIE	Commission Internationale de l'Eclairage
KAS	Kissinger-Akahira-Sunose
FWO	Flynn-Wall-Ozawa
Vyazovkin AIC	Vyazovkin Advanced isoconversional
TGA	Thermogravimetric analysis
β	Heating rate
α	Conversion point
J ₀	Kinetic barrier of nucleation
J	Nucleation rate
T _P	Peak temperature
K _B	Boltzmann constant
E α	Activation energy of nucleation
A α	Pre-exponential kinetic factor
ΔH	Change in enthalpy
ΔG	Change in Gibbs free energy
ΔS	Change in entropy
f(α)	Differential function
g(α)	Integral function
Exp ($\Delta G/RT$)	Thermodynamic barrier
M ₀	Initial weight of Gd ₂ O ₃ before TGA
M _f	Final weight of Gd ₂ O ₃ after TGA
R	Universal gas constant
Z(α)	Product of differential and integral function
h	Plank constant

FWHM	Full-width half maxima
XPS	X-ray photoelectron spectroscopy
XRD	X-ray diffraction
FTIR	Fourier-transform infrared spectroscopy
HRTEM	High-resolution transmission electron microscopy

PREFACE AND THESIS ORGANIZATION

Recently, biomedical imaging technologies have been widely used for early disease identification and diagnosis. Several imaging modalities, including computed tomography (CT), magnetic resonance imaging (MRI), photoacoustic imaging (PAI), positron emission tomography (PET), single-photon-emission computed tomography (SPECT), and optical imaging (OI), play important roles in the observation of biological system structures and functions and provide important information about the pathogenesis, progression, and treatment of diseases such as cancer. Because of their relative drawbacks, monomodal imaging techniques typically cannot achieve the requirements of high sensitivity and spatial resolution. As a result, combining two or more imaging modalities, known as dual or multimodal imaging, is a common technique to circumvent these constraints. Nowadays, merging diverse components into a single platform is the most frequent technique for utilizing their unique functions. The complicated components impede this strategy and synthetic procedure, causing inevitable interference, poor reproducibility, and uncertain pharmacokinetics, and hence less accessible for clinical use. Alternatively, one component with multiple contrasting capacities remains more desirable due to the lower interference, simpler fabrication, defined structures, and far better reproducibility than the composite agents. In this thesis work, we exclusively developed a novel platform for the synthesis of nanoparticles for multimodal imaging (MRI and fluorescent imaging) by a one-pot facile synthetic route. Surface functionalization with commercially available polymer bovine serum albumin and chitosan enables precise control over size and makes nanomaterial biocompatible. Developed nanoprobes were characterized by several microscopic and spectroscopic techniques to confirm the synthesis of ultras-small Gd_2O_3 nanoclusters. Furthermore, post-characterization studies such as *in-vitro* and *in-vivo* biocompatibility,

hemocompatibility, real-time imaging in mice, *in-vitro* imaging in HaCaT cells (Human keratinocytes), and U-87 MG (Human glioblastoma cells), and in-vitro relaxivity measurement suggested it as a potential contrast agent and confirmed its candidature toward multimodal imaging.

The current thesis work is divided into six chapters.

Chapter 1 of the thesis covered a detailed description of multimodal imaging techniques and their advantages and disadvantages. It also provides insight into their multidimensional applications in disease prognosis. This chapter provides the details of contrast agents and discusses various synthetic routes to synthesize Gd₂O₃ nanomaterials for imaging purposes. This chapter also provides a detailed discussion of capping agents used in the synthesis of Gd₂O₃ nanomaterials.

Chapter 2 consists of an extensive literature survey on the synthetic approach and multifunctional aspects of Gd₂O₃-based nanomaterials. This chapter also gives insight into the effect of texture, shape, and size effect of Gd₂O₃ nanomaterials on its properties and prospective application. The literature survey also addresses the possible applications of the Gd₂O₃ nanomaterials in the biomedical field. In addition, this study also addresses the importance and associated challenges with determining the nucleation rate and interfacial energy at elevated temperatures, as well as the corresponding conversions.

Chapter 3 explains a facile one-pot novel technique to synthesize water-soluble multifluorescent Gd₂O₃ nanoclusters by utilizing BSA protein and ascorbic acid as capping and reducing agents, respectively. The prepared clusters exhibited tunable fluorescence, high quantum yield, excellent photostability, wide-range pH, and ionic strength tolerability. These multifunctional properties of Gd₂O₃ nanoclusters are availed in labelling HaCaT cell lines with negligible toxicity.

Chapter 4 of the thesis reports a novel strategy to compute various parameters such as activation energy, preexponential factor, nucleation rate, interfacial energy, and thermodynamic parameters of Gd_2O_3 nanoclusters using non-isoconversional thermogravimetric models at high temperatures. The Vyazovkin AIC method was utilized to estimate activation energy, which was found to be 143.98 kJ/mol. In this work, we proposed four different models for calculating nucleation rate and interfacial energy.

Chapter 5 provides the one-pot facile synthesis of Gd_2O_3 nanoclusters using a chitosan polymer template. The prepared Gd_2O_3 clusters show a wide range of emissions range without mixing any dopants. The prepared clusters exhibit negligible cytotoxicity, excellent water dispersibility, prolonged photostability, and high absolute quantum yield. The prepared clusters exhibit high longitudinal relaxation along with luminous properties and hence could be applied in both MR imaging and fluorescence imaging. Besides the *in vitro* study, this chapter includes real-time rodent imaging using an IVIS (*in-vivo* imaging system), hemocompatibility assay, and *in-vivo* toxicological study.

Chapter 6 of the thesis summarizes the whole study in a nutshell with the future prospects of prepared nanoclusters in various fields and highlights the major upshot of every chapter for achieving the objective of the whole study in a collaborative manner. The composition reported in this study primarily focused on developing novel nanoplatforms for multimodal imaging applications by functionalizing them with different capping agents. The current work is envisioned to contribute significantly in the areas of science, engineering, and nanomedicine with targeted drug delivery.